

# Quantum capacitance of an HgTe quantum well as an indicator of the topological phase

T. Kernreiter, M. Governale, and U. Zülicke

*School of Chemical and Physical Sciences and MacDiarmid Institute for Advanced Materials and Nanotechnology, Victoria University of Wellington, PO Box 600, Wellington 6140, New Zealand*

(Dated: November 6, 2018)

Varying the quantum-well width in an HgTe/CdTe heterostructure allows to realize normal and inverted semiconducting band structures, making it a prototypical system to study two-dimensional (2D) topological-insulator behavior. We have calculated the zero-temperature thermodynamic density of states  $D_T$  for the electron-doped situation in both regimes, treating interactions within the Hartree-Fock approximation. A distinctively different behavior for the density dependence of  $D_T$  is revealed in the inverted and normal cases, making it possible to detect the system's topological phase through measurement of macroscopic observables such as the quantum capacitance or electronic compressibility. Our results establish the 2D electron system in HgTe quantum wells as unique in terms of its collective electronic properties.

PACS numbers: 73.21.Fg, 71.45.Gm, 73.20.At

*Introduction.*—Capacitance measurements are a premier tool to elucidate the electronic properties of two-dimensional (2D) electron systems [1–14]. They fundamentally probe the thermodynamic density of states,

$$D_T = \frac{\partial n}{\partial \mu} \quad , \quad (1)$$

where  $n$  and  $\mu$  denote the 2D system's electronic sheet density and chemical potential, respectively. More specifically,  $D_T$  is related to the quantum capacitance per unit area  $C_q$  and the electronic compressibility  $K$  via

$$C_q = e^2 D_T \quad , \quad (2a)$$

$$K = \frac{D_T}{n^2} \quad . \quad (2b)$$

The intriguing interplay between single-particle and Coulomb-interaction contributions to  $D_T$  has been intensely studied theoretically, both for conventional 2D electron systems realized in heterostructures [15–18] and few-layer graphene [18–22]. In particular, the tendency towards negative electronic compressibility in the low-density limit [23] has attracted a lot of attention [3–9].

Here we show how the thermodynamic density of states of electrons in an HgTe quantum well exhibits behavior different from any of the previously studied 2D electron systems, essentially because of the anomalous properties of an interaction-related inter-band contribution relevant for narrow-gap systems. Our work provides new insight complementing the observation of unusual electric-transport properties in this system [24–27] that relate to the existence of an unconventional, inverted, 2D electronic band structure when the quantum-well width  $d$  is larger than a critical value  $d_c \approx 6.3$  nm [28–31]. The deeper understanding derived from our results also enables novel characterization of topological phases [32] in other 2D [33, 34] and bulk [32, 35] materials and extends the general knowledge about unusual collective properties of topological and Dirac-semimetal systems [36–38].

We calculate the thermodynamic density of states for electrons in HgTe quantum wells, taking Coulomb interactions into account within the Hartree-Fock approximation. To be specific, we focus on two experimentally feasible situations with quantum-well widths  $d = 5$  nm and 7 nm, respectively, and present predictions for  $D_T$  as a function of the 2D-system's Fermi wave vector. In our calculations, crucial effects arising from the finite width of electronic bound states in the HgTe/CdTe heterostructure are included. Quite generally, we find that interaction contributions significantly affect  $D_T$  and, thus, observables such as the quantum capacitance and the electronic compressibility. See Fig. 1 for a pertinent example. More specifically, it turns out that the inter-band exchange correction depends strongly on the quantum-well width and changes its sign for a value close to  $d_c$ .

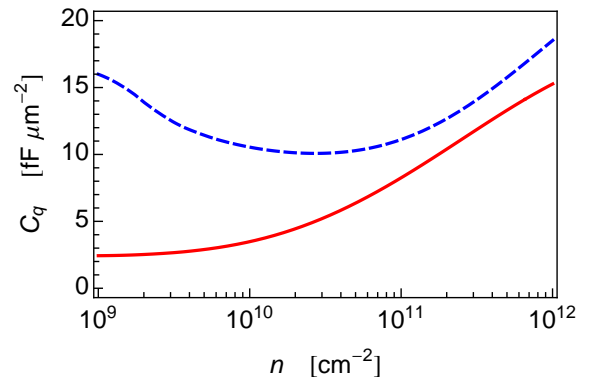


FIG. 1. Density dependence of the quantum capacitance per unit area for electrons in an HgTe quantum well. The red solid (blue dashed) curve is obtained for a quantum-well width  $d = 7$  nm (5 nm) corresponding to the topological (normal) situation. Clearly distinguishable opposite trends emerge in the low-density regime.

We elucidate the underlying mechanisms such as the interplay of band-structure parameters that lead to this interesting behavior.

*Model and Formalism.*—The theoretical framework for our calculation of many-particle effects for electrons in an HgTe quantum well is based on the BHZ Hamiltonian [28]. The latter adequately describes the relevant single-particle states in the low-energy band structure, using basis functions  $|E_{1\pm}\rangle$ , which are superposition of conduction-electron and light-hole (LH) states, and the heavy-hole (HH) states  $|H_{1\pm}\rangle$ . Within the representation defined by the basis-state vector ( $|E_{1+}\rangle, |H_{1+}\rangle, |E_{1-}\rangle, |H_{1-}\rangle$ ), the BHZ Hamiltonian is block-diagonal and given by

$$\mathcal{H}_0 = \begin{pmatrix} \mathcal{H}^{(+)} & 0 \\ 0 & \mathcal{H}^{(-)} \end{pmatrix}, \quad (3)$$

with  $\mathcal{H}^{(s)} = h_{\mu}^{(s)} \sigma^{\mu}$ ,  $h^{(s)} = (C - Dk^2, sAk_x, -Ak_y, M - Bk^2)$  and  $\sigma^{\mu} = (\mathbb{1}, \sigma_x, \sigma_y, \sigma_z)$  where  $\sigma_j$  are the Pauli matrices. The quantum number  $s = \pm 1$  distinguishes spin-1/2 projections parallel to the quantum-well growth direction, and the effective band-structure parameters  $A, B, C, D, M$  are functions of the quantum-well width  $d$  [39]. For simplicity, we set the irrelevant overall energy shift  $C$  to zero. The sign of the gap parameter  $M$  distinguishes the ordinary and inverted-band situations: using the convention  $B < 0$ , the system is in the topological (normal) regime when  $M < 0$  ( $M > 0$ ).

The energy eigenvalues of the BHZ Hamiltonian (3)

are given by [28]

$$E_{\mathbf{k}\alpha}^{(s)} \equiv E_{k\alpha}^{(s)} = -Dk^2 + \alpha \sqrt{(M - Bk^2)^2 + A^2 k^2}, \quad (4)$$

where  $\alpha = \pm 1$  distinguishes conduction and valence bands, both of which are doubly degenerate in  $s$ . Due to the inherent axial symmetry of the BHZ model, the eigenvectors of the two  $2 \times 2$  matrices  $\mathcal{H}^{(s)}$  in Eq. (3) can be expressed as  $a_{\mathbf{k}\alpha}^{(s)} = U_{\phi_{\mathbf{k}}}^{(s)} a_{k\alpha}^{(s)}$  in terms of the polar coordinates  $(k, \phi_{\mathbf{k}})$  for wave vector  $\mathbf{k}$ , with

$$a_{k\alpha}^{(s)} = \frac{1}{\sqrt{2}} \begin{pmatrix} \alpha \left[ 1 - \frac{\alpha(Bk^2 - M)}{\sqrt{A^2 k^2 + (Bk^2 - M)^2}} \right]^{\frac{1}{2}} \\ s \left[ 1 + \frac{\alpha(Bk^2 - M)}{\sqrt{A^2 k^2 + (Bk^2 - M)^2}} \right]^{\frac{1}{2}} \end{pmatrix} \quad (5)$$

and  $U_{\phi_{\mathbf{k}}}^{(s)} = \text{diag}(e^{is\phi_{\mathbf{k}}/2}, e^{-is\phi_{\mathbf{k}}/2})$ .

*Quantum many-body effects.*—The single-particle band dispersions given in Eq. (4) are renormalized by interaction effects. Assuming that the electrostatic (Hartree) terms are compensated by the influence of a neutralizing background charge density, we focus here on the exchange (Fock) contributions. The fundamental quasi-2D character of the charge carriers is accounted for by retaining the full  $z$  dependence of quantum-well bound states through the basis functions  $|E_{1+}\rangle, |H_{1+}\rangle, |E_{1-}\rangle, |H_{1-}\rangle$  for the BHZ Hamiltonian. The Fock self-energy of conduction-band electrons can then be written as

$$\Sigma_{k\pm}^{(s)} = -2\pi C \int \frac{d^2 k'}{(2\pi)^2} n_{\text{F}}(E_{\mathbf{k}'\pm}^{(s)}) \int dz \int dz' \frac{e^{-|\mathbf{k}-\mathbf{k}'||z-z'|}}{|\mathbf{k}-\mathbf{k}'|} \left[ \psi_{\mathbf{k}'\pm}^{(s)}(z)^\dagger \cdot \psi_{\mathbf{k}\pm}^{(s)}(z) \right] \left[ \psi_{\mathbf{k}\pm}^{(s)}(z')^\dagger \cdot \psi_{\mathbf{k}'\pm}^{(s)}(z') \right], \quad (6)$$

where  $C = e^2/(4\pi\epsilon_0)$  measures the Coulomb-interaction strength,  $n_{\text{F}}(E)$  is the Fermi function, and the  $\psi_{\mathbf{k}\alpha}^{(s)}(z)$  are six-dimensional spinor wave functions comprising the bands with  $\Gamma_6$  and  $\Gamma_8$  symmetry closest to the bulk-material's fundamental gap [40]. Intra-(inter-)band contributions to the Fock self-energy are labeled by the subscript  $+$  ( $-$ ). Note that terms with  $s \neq s'$  vanish for the block-diagonal BHZ model given above because of the orthogonality of the associated basis states. However, such contributions do arise when spin-orbit-coupling effects are included. Effects of the latter will be discussed briefly at the end of this paper.

In the zero-temperature limit, which we consider in the following, the Fermi functions in Eq. (6) reduce to  $n_{\text{F}}(E_{\mathbf{k}-}^{(s)}) = 1$  for the fully occupied valence band and  $n_{\text{F}}(E_{\mathbf{k}+}^{(s)}) = \Theta(k_{\text{F}} - |\mathbf{k}|)$ , where  $k_{\text{F}}$  is the modulus of the Fermi wave vector for electrons in the conduction band, and  $\Theta(\cdot)$  denoted the Heaviside step function. To take

into account both the in-plane dynamics described by the BHZ Hamiltonian as well as the nontrivial spinor structure of the BHZ-model basis states, we employ subband  $\mathbf{k} \cdot \mathbf{p}$  theory [41, 42] to write the spinor wave functions  $\psi_{\mathbf{k}\alpha}^{(s)}(z)$  as superpositions

$$\psi_{\mathbf{k}\alpha}^{(s)}(z) = \sum_{i=1}^2 \left( U_{\phi_{\mathbf{k}}}^{(s)} \right)_{ii} a_{k\alpha,i}^{(s)} \psi_{0i}^{(s)}(z), \quad (7)$$

where the coefficients  $a_{k\alpha,i}^{(s)}$  are the components of the corresponding eigenvectors, Eq. (5), of the BHZ Hamiltonian. The six-dimensional spinors  $\psi_{0i}^{(s)}(z)$  are the BHZ-model basis-state spinors for zero in-plane wave vector, which are determined by the solutions to a confined-particle problem for the HgTe/CdTe quantum-well heterostructure. Their explicit expressions have been given in the supplemental information of Ref. [28], where for instance  $\psi_{01}^{(+)}(z)^T = (f_1(z), 0, 0, f_4(z), 0, 0)$  and

$\psi_{02}^{(+)}(z)^T = (0, 0, f_3(z), 0, 0, 0)$  which are normalized, i.e.,  $\int dz |\psi_{0i}^{(s)}(z)|^2 = 1, \forall i, s$ . As a result, we obtain for the intra- and inter-band contributions to the Fock self-energy

$$\begin{aligned} \Sigma_{k_{\pm}}^{(s)} &= \frac{-C}{\pi} \int_0^\pi d\phi \int_0^{k_{\pm}} dk' k' \int dz \int dz' \frac{e^{-r(k, k', \phi)|z-z'|}}{r(k, k', \phi)} \\ &\times \sum_{i,j} \mathcal{F}_{ij}(\phi) a_{k'_{\pm}, i}^{(s)} a_{k'_{\pm}, j}^{(s)} a_{k_{\pm}, i}^{(s)} a_{k_{\pm}, j}^{(s)} |\psi_{0i}^{(s)}(z)|^2 |\psi_{0j}^{(s)}(z')|^2, \end{aligned} \quad (8)$$

where the integration limits are  $k_+ = k_F$  (intra-band) and  $k_- = k_c$  (inter-band), with  $k_c$  being an ultraviolet cutoff. In Eq. (8),  $r(k, k', \phi) = \sqrt{k^2 + k'^2 - 2kk' \cos \phi}$  and  $\mathcal{F}_{ij}(\phi) = \sqrt{1 - (1 - \delta_{ij}) \sin^2 \phi}$ , with  $\phi \equiv \phi_{\mathbf{k}} - \phi_{\mathbf{k}'}$  and  $\delta_{ij}$  being the Kronecker symbol. The inter-band contribution depends logarithmically on  $k_c$ , which is typically chosen to be of the order of the inverse lattice constant [19, 20]. Finally, with the chemical potential given in terms of  $k_F$  as  $\mu = E_{k_F+}^{(s)} + \Sigma_{k_F+}^{(s)} + \Sigma_{k_F-}^{(s)}$ , and using the relation  $n = k_F^2/(2\pi)$ , the expression (1) for the thermodynamic density of states can be rewritten as  $D_T = \left( \frac{\pi}{k_F} \frac{\partial \mu}{\partial k_F} \right)^{-1}$ . Measuring wave vectors and energies in terms of the BHZ-model scales  $q_0 \equiv A/|B|$  and  $E_0 \equiv Aq_0$ , the natural unit for  $D_T^{-1}$  is  $|B|$ . The fine-structure constant that appears in the exchange-energy contributions to  $\mu$  is given by  $\alpha_{\text{qw}} \equiv e^2/(4\pi\epsilon\epsilon_0 A) \approx 0.19$  when using  $\epsilon = 20.8$  as the dielectric constant of HgTe.

*Numerical results for  $D_T$ .*—We now present results obtained for the thermodynamic density of states in normal and topological HgTe quantum wells. Following the usual convention,  $D_T^{-1} \equiv \partial\mu/\partial n$  is shown as a function of the Fermi wave vector. We first consider an HgTe quantum well with width  $d = 5$  nm, which is in the normal (non-inverted band-structure) regime. The associated BHZ parameters are given in Table I and correspond to an actual experimental realization [39]. For the large-momentum cutoff of the inter-band contribution, we choose  $k_c = a_0^{-1}$ , with  $a_0 = 0.646$  nm being the HgTe bulk-material lattice constant. We show the result obtained for  $D_T^{-1}$  in Fig. 2, making also explicit the various contributions to  $D_T^{-1}$ . The purely kinetic (i.e., noninteracting) part is given by a constant in the low-density

	$d = 5$ nm	$d = 7$ nm
$A$ [eV nm]	0.365	0.340
$B$ [eV nm <sup>2</sup> ]	-0.50	-0.50
$D$ [eV nm <sup>2</sup> ]	-0.50	-0.87
$M$ [meV]	24.0	-8.5

TABLE I. Parameters of the BHZ model applicable for two experimental realizations of HgTe quantum wells [39] having widths  $d = 5$  nm and 7 nm, respectively.

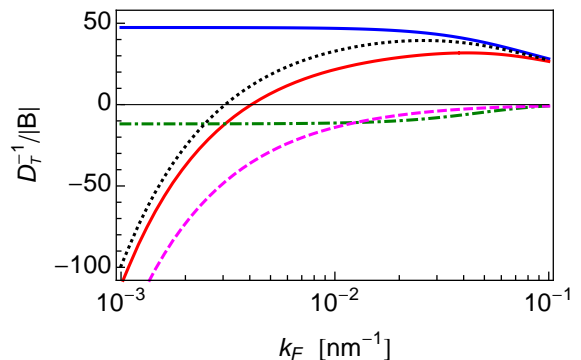


FIG. 2. Inverse thermodynamic density of states  $D_T^{-1} \equiv \partial\mu/\partial n$  of an HgTe quantum well in the normal regime (well width  $d = 5$  nm). The red (blue) solid curve shows the result with (without) interactions. The magenta dashed (green dot-dashed) curve is the intra-band (inter-band) exchange contribution only. The black dotted curve is the sum of the noninteracting and intra-band exchange contributions.

regime,

$$\left. \frac{\partial E_{k_F\alpha}^{(s)}}{\partial n} \right|_{k_F=0} = 2\pi \left[ \alpha \left( \frac{A^2}{2|M|} + |B| \text{sign}(M) \right) - D \right], \quad (9)$$

which has the form expected for an ordinary 2D electron system [43]. However, it exhibits a weak dependence on  $k_F$  at larger carrier densities due to the HH-LH mixing of quantum-well bound states having finite in-plane wave vector. The intra-band interaction (Fock) renormalization term is always negative and therefore reduces  $D_T^{-1}$ , thus leading to an enhancement of the electronic compressibility. At low-enough densities, the intra-band contribution drives  $D_T^{-1}$  to negative values. Such a behavior is also reminiscent of that of an ordinary 2D electron system [44]. In the normal regime (except very close to the critical well width  $d_c$ ), the inter-band exchange contribution is also negative and thus reduces  $D_T^{-1}$  further. As a result, the crossover from positive to negative values of  $D_T^{-1}$  is shifted to higher densities. This behaviour has to be contrasted to that exhibited by single-layer graphene where the exchange renormalization of  $D_T^{-1}$  is positive [19, 20]. Overall, from the results shown in Fig. 2, we see that the exchange contributions strongly influence the electronic compressibility.

We now consider the inverted regime of an HgTe quantum well, which is realized for a well width  $d > d_c \approx 6.3$  nm. Taking the BHZ parameters of a feasible experimental situation corresponding to a well width  $d = 7$  nm (see Table I), we again calculate the quantity  $D_T^{-1}$ . The result is shown in Fig. 3. The most salient feature is that the inter-band exchange contribution is now *positive*, like in single-layer graphene [19, 20], and considerably larger in magnitude as compared to the situation in the normal regime. In contrast, the intra-band exchange term is of similar magnitude and has the same sign as in the normal

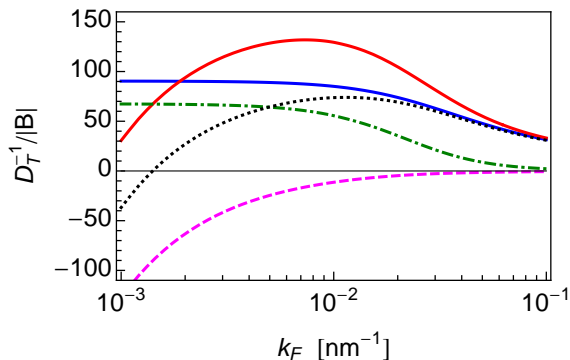


FIG. 3. Inverse thermodynamic density of states  $D_T^{-1} \equiv \partial\mu/\partial n$  of an HgTe quantum well in the inverted regime (well width  $d = 7$  nm). The red (blue) solid curve shows the result with (without) interactions. The magenta dashed (green dot-dashed) curve is the intra-band (inter-band) exchange contribution only. The black dotted curve is the sum of the noninteracting and intra-band exchange contributions. Notice the opposite sign of the inter-band exchange contribution (green dot-dashed curve), which shifts the crossover to negative compressibility to very low carrier densities.

case. The kinetic (noninteracting) contribution is much larger as compared to the  $d = 5$ -nm case, which is mainly due to the smaller band gap in the present case — this can be inferred from Eq. (9). We see that the electronic compressibility is reduced by up to 35% due to exchange effects as compared with the noninteracting case. This trend is changed only at very low densities where the (negative) intra-band contribution becomes dominant.

The striking difference observed between the inter-band interaction-renormalization contributions in the topological and normal regimes invites more detailed scrutiny. Figure 4 illustrates the variation of intra-band and inter-band exchange terms as a function of the quantum-well width [45] for a fixed carrier density  $n = 10^{10} \text{ cm}^{-2}$ . The intra-band contribution is always negative and rather insensitive to a variation of  $d$ . The inter-band contribution, however, depends strongly on the quantum-well width and changes its sign in the vicinity of the critical value  $d_c \approx 6.3$  nm. Also around  $d_c$ , due to the vanishing band gap, we can anticipate the onset of a divergence in the inter-band contribution for  $k_F \rightarrow 0$ . Figure S1 in the Supplemental Material shows this even more clearly. We can attribute the sign change in the inter-band exchange contribution to  $D_T^{-1}$  to a complex interplay of band-mixing effects (due to the terms proportional to  $A$  in the BHZ Hamiltonian) and the change of the band characters when crossing over from  $M > 0$  to  $M < 0$ . To be more specific, we find that the heavy-hole term ( $i = j = 2$ ) in Eq. (8) gives generally (especially for low densities) the largest contribution to  $\Sigma_{k_F-}^{(s)}$  (as well as to  $\partial\Sigma_{k_F-}^{(s)}/\partial n$ ), where for  $M > 0$  ( $M < 0$ ) it is a monotonically decreasing (increasing) function of  $k_F$ .

*Effect of spin-orbit coupling.*—We have extended our

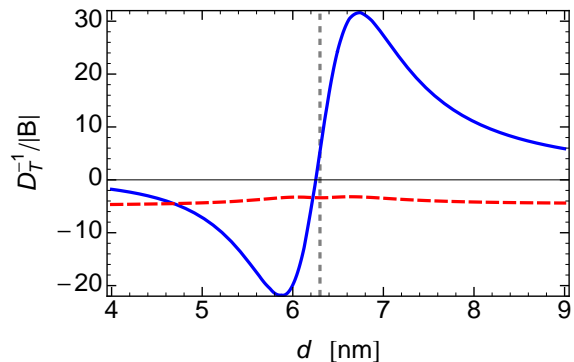


FIG. 4. Intra-band (dashed red curve) and inter-band (solid blue curve) exchange contribution to the inverse thermodynamic density of states  $D_T^{-1}$  as a function of the HgTe quantum-well width  $d$  for carrier sheet density  $n = 10^{10} \text{ cm}^{-2}$ . The dashed vertical line indicates the value of the critical well width  $d_c = 6.3$  nm.

calculation of the thermodynamic density of states to the situation with bulk-inversion-asymmetry and structural-inversion-asymmetry spin-orbit coupling [29, 46] and find that, only for the largest expected magnitudes of the bulk-inversion-asymmetry energy scale of a few meV, results change quantitatively by upto 10%. However, our findings suggest that spin-orbit coupling affects the electronic compressibility of electrons in HgTe quantum wells typically only at the percent level. See the Supplemental Material for more details.

*Conclusions.*—We have presented results for the thermodynamic density of states for electrons in HgTe quantum wells in experimentally feasible situations. Interaction effects have been included within the Hartree-Fock approximation. We have also taken into account the finite width of the HgTe/CdTe quantum-well heterostructure, which is necessary to account for the attenuated Coulomb repulsion in the transverse direction. Markedly different behavior is exhibited for a well width of  $d = 5$  nm (normal regime) compared to one with  $d = 7$  nm (topological regime). We have pinpointed the origin of this finding as the sizeable inter-band exchange correction whose sign differs in the topological and normal regimes. Thus a measurement of the quantum capacitance of HgTe quantum wells, e.g. using HgTe double-quantum-well configurations [47], provides a useful way to determine the topological state of this system.

The enhancement and eventual sign change of the compressibility found in the low-density limit of the non-topological phase is analogous to the behavior exhibited by ordinary 2D electron systems with parabolic dispersion [3–9]. In contrast, the compressibility of the 2D electron system in the topological phase is strongly suppressed by Coulomb interactions. Additional contributions to the compressibility arising from image charges [16, 17] and disorder [48] can be straightforwardly included to facilitate the description of real samples.

- 
- [1] T. P. Smith, B. B. Goldberg, P. J. Stiles, and M. Heiblum, *Phys. Rev. B* **32**, 2696 (1985).
- [2] S. Luryi, *Appl. Phys. Lett.* **52**, 501 (1988).
- [3] S. V. Kravchenko, D. A. Rinberg, S. G. Semenchinsky, and V. M. Pudalov, *Phys. Rev. B* **42**, 3741 (1990).
- [4] J. P. Eisenstein, L. N. Pfeiffer, and K. W. West, *Phys. Rev. Lett.* **68**, 674 (1992).
- [5] J. P. Eisenstein, L. N. Pfeiffer, and K. W. West, *Phys. Rev. B* **50**, 1760 (1994).
- [6] S. Shapira, U. Sivan, P. M. Solomon, E. Buchstab, M. Tischler, and G. Ben Yoseph, *Phys. Rev. Lett.* **77**, 3181 (1996).
- [7] I. S. Millard, N. K. Patel, C. L. Foden, E. H. Linfield, M. Y. Simmons, D. A. Ritchie, and M. Pepper, *Phys. Rev. B* **55**, 6715 (1997).
- [8] S. C. Dultz and H. W. Jiang, *Phys. Rev. Lett.* **84**, 4689 (2000).
- [9] G. Allison, E. A. Galaktionov, A. K. Savchenko, S. S. Safonov, M. M. Fogler, M. Y. Simmons, and D. A. Ritchie, *Phys. Rev. Lett.* **96**, 216407 (2006).
- [10] J. Martin, N. Akerman, G. Ulbricht, T. Lohmann, J. H. Smet, K. von Klitzing, and A. Yacoby, *Nat. Phys.* **4**, 144 (2008).
- [11] E. A. Henriksen and J. P. Eisenstein, *Phys. Rev. B* **82**, 041412 (2010).
- [12] L. Li, C. Richter, S. Paetel, T. Kopp, J. Mannhart, and R. C. Ashoori, *Science* **332**, 825 (2011).
- [13] A. F. Young, C. R. Dean, I. Meric, S. Sorgenfrei, H. Ren, K. Watanabe, T. Taniguchi, J. Hone, K. L. Shepard, and P. Kim, *Phys. Rev. B* **85**, 235458 (2012).
- [14] D. A. Kozlov, D. Bauer, J. Ziegler, R. Fischer, M. L. Savchenko, Z. D. Kvon, N. N. Mikhailov, S. A. Dvoretzky, and D. Weiss, *Phys. Rev. Lett.* **116**, 166802 (2016).
- [15] G. Giuliani and G. Vignale, *Quantum Theory of the Electron Liquid* (Cambridge U Press, Cambridge, UK, 2005) See also the early work by M. S. Bello, E. I. Levin, B. I. Shklovskii and A. L. Efros, *Zh. Eksp. Teor. Fiz.* **80**, 1596 (1981) [*Sov. Phys. JETP* **53**, 822 (1981)].
- [16] B. Skinner and B. I. Shklovskii, *Phys. Rev. B* **82**, 155111 (2010).
- [17] B. Skinner and M. M. Fogler, *Phys. Rev. B* **82**, 201306 (2010).
- [18] Q. Li, E. H. Hwang, and S. Das Sarma, *Phys. Rev. B* **84**, 235407 (2011).
- [19] E. H. Hwang, B. Y.-K. Hu, and S. Das Sarma, *Phys. Rev. Lett.* **99**, 226801 (2007).
- [20] S. V. Kusminskiy, J. Nilsson, D. K. Campbell, and A. H. Castro Neto, *Phys. Rev. Lett.* **100**, 106805 (2008).
- [21] G. Borghi, M. Polini, R. Asgari, and A. H. MacDonald, *Phys. Rev. B* **82**, 155403 (2010).
- [22] D. S. L. Abergel, E. H. Hwang, and S. Das Sarma, *Phys. Rev. B* **83**, 085429 (2011).
- [23] B. Tanatar and D. M. Ceperley, *Phys. Rev. B* **39**, 5005 (1989).
- [24] M. König, S. Wiedmann, C. Brüne, A. Roth, H. Buhmann, L. W. Molenkamp, X. Qi, and S. Zhang, *Science* **318**, 766 (2007).
- [25] A. Roth, C. Brüne, H. Buhmann, L. W. Molenkamp, J. Maciejko, X. Qi, and S. Zhang, *Science* **325**, 294 (2009).
- [26] C. Brüne, A. Roth, H. Buhmann, E. M. Hankiewicz, L. W. Molenkamp, J. Maciejko, X. Qi, and S. Zhang, *Nat. Phys.* **8**, 485 (2012).
- [27] S. Hart, H. Ren, M. Kosowsky, G. Ben-Shach, P. Leubner, C. Brüne, H. Buhmann, L. W. Molenkamp, B. I. Halperin, and A. Yacoby, preprint arXiv:1509.02940.
- [28] B. A. Bernevig, T. L. Hughes, and S. Zhang, *Science* **314**, 1757 (2006).
- [29] M. König, H. Buhmann, L. W. Molenkamp, T. Hughes, C.-X. Liu, X.-L. Qi, and S.-C. Zhang, *J. Phys. Soc. Jpn.* **77**, 031007 (2008).
- [30] R. Winkler, L. Wang, Y. Lin, and C. Chu, *Solid State Commun.* **152**, 2096 (2012).
- [31] S. A. Tarasenko, M. V. Durnev, M. O. Nestoklon, E. L. Ivchenko, J.-W. Luo, and A. Zunger, *Phys. Rev. B* **91**, 081302 (2015).
- [32] X. Qi and S. Zhang, *Rev. Mod. Phys.* **83**, 1057 (2011).
- [33] C. Liu, T. L. Hughes, X. Qi, K. Wang, and S. Zhang, *Phys. Rev. Lett.* **100**, 236601 (2008).
- [34] I. Knez, R. Du, and G. Sullivan, *Phys. Rev. Lett.* **107**, 136603 (2011).
- [35] M. Z. Hasan and J. E. Moore, *Annu. Rev. Condens. Matter Phys.* **2**, 55 (2011).
- [36] S. Juergens, P. Michetti, and B. Trauzettel, *Phys. Rev. Lett.* **112**, 076804 (2014).
- [37] S. Juergens, P. Michetti, and B. Trauzettel, *Phys. Rev. B* **90**, 115425 (2014).
- [38] T. Kernreiter, M. Governale, U. Zülicke, and E. M. Hankiewicz, *Phys. Rev. X* **6**, 021010 (2016).
- [39] M. Mühlbauer, A. Budewitz, B. Büttner, G. Tkachov, E. M. Hankiewicz, C. Brüne, H. Buhmann, and L. W. Molenkamp, *Phys. Rev. Lett.* **112**, 146803 (2014).
- [40] R. Winkler, *Spin-Orbit Coupling Effects in Two-Dimensional Electron and Hole Systems* (Springer, Berlin, 2003).
- [41] D. A. Broido and L. J. Sham, *Phys. Rev. B* **31**, 888 (1985).
- [42] S.-R. E. Yang, D. A. Broido, and L. J. Sham, *Phys. Rev. B* **32**, 6630 (1985).
- [43] The r.h.s. of Eq. (9) can be expressed as  $\pi\hbar^2/m_*$ , where  $m_*$  is the effective band mass of 2D electrons obtained from the small- $k$  expansion of the dispersion (4).
- [44] The intra-band Fock contribution to  $D_T^{-1}$  diverges  $\propto k_F^{-1}$  in the low-density limit like the Fock contribution for an ordinary 2D electron gas [17]. In real samples, this divergence is cut off by image-charge effects [16, 17].
- [45] The BHZ parameters  $A$  and  $B$  are generally only weakly dependent on the HgTe quantum-well width  $d$  (see Table I) and, for this calculation, we use the  $A$  and  $B$  values for  $d = 7$  nm. The mass parameter  $M$ , on the other hand, depends sensitively on  $d$ , and we extract its functional dependence from the band-edge energies of the conduction and valence bands, which are obtained by appropriate matching conditions derived from the relevant confined-electron problem (see the supplemental information of Ref. 28). Note that the BHZ parameter  $D$  does not enter the exchange corrections to  $D_T^{-1}$ .
- [46] D. G. Rothe, R. W. Reithaler, C.-X. Liu, L. W. Molenkamp, S.-C. Zhang, and E. M. Hankiewicz, *New J. Phys.* **12**, 065012 (2010).
- [47] M. V. Yakunin, A. V. Suslov, M. R. Popov, E. G. Novik, S. A. Dvoretzky, and N. N. Mikhailov, *Phys. Rev. B* **93**, 085308 (2016).
- [48] M. M. Fogler, *Phys. Rev. B* **69**, 121409 (2004).

**SUPPLEMENTAL MATERIAL FOR "QUANTUM  
CAPACITANCE OF AN HGTE QUANTUM  
WELL AS AN INDICATOR OF THE  
TOPOLOGICAL PHASE"**

**INTER-BAND SELF-ENERGY CONTRIBUTION**

We show in Fig. S1 the inter-band Fock contribution to  $D_T^{-1}$  for three different densities  $n = (5 \times 10^9, 10^{10}, 5 \times 10^{10}) \text{ cm}^{-2}$ . Especially for lower densities, it can be clearly seen that the inter-band contribution changes its sign close to the critical value  $d_c \approx 6.3 \text{ nm}$ . For higher densities, however, the crossover occurs at somewhat smaller values of  $d$ . The reason for this tendency can be traced to the fact that, for larger densities, other terms besides the dominant HH-related contributions become important in the sum in Eq. (8).

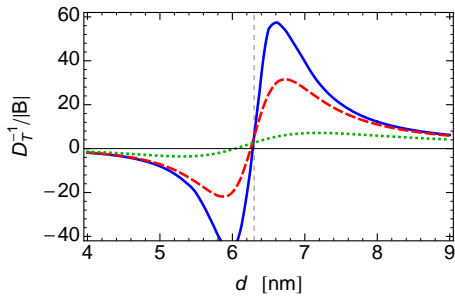


FIG. S1. Inter-band exchange contribution to the inverse thermodynamic density of states  $D_T^{-1}$  as a function of the HgTe quantum-well width  $d$  for carrier sheet densities  $n = 5 \times 10^9 \text{ cm}^{-2}$  (blue solid curve),  $10^{10} \text{ cm}^{-2}$  (red dashed curve), and  $5 \times 10^{10} \text{ cm}^{-2}$  (green dotted curve). The dashed vertical line indicates the value of the critical well width  $d_c = 6.3 \text{ nm}$ .

**EFFECTS OF SPIN-ORBIT COUPLING**

Spin-orbit coupling due to structural inversion asymmetry (SIA) and bulk inversion asymmetry (BIA) can be straightforwardly incorporated into the BHZ Hamiltonian. In the following, we discuss the influence of those types of spin-orbit coupling separately.

*SIA.* The leading contribution due to SIA arising from the presence of a perpendicular electric field  $\mathcal{E}_z$  is linear in the wave vector and given by [46]

$$\mathcal{H}_R = \begin{pmatrix} 0 & 0 & -iR_0k_- & 0 \\ 0 & 0 & 0 & 0 \\ iR_0k_+ & 0 & 0 & 0 \\ 0 & 0 & 0 & 0 \end{pmatrix}. \quad (\text{S1})$$

Typical values are  $R_0/(e\mathcal{E}_z) = -15.6 \text{ nm}^2$  [46] and  $\mathcal{E}_z = 0.01 \text{ V nm}^{-1}$  [27]. We define the SIA-related dimensionless parameter  $\xi_R \equiv |R_0/A|$  ( $\approx 0.44$  in a typical HgTe

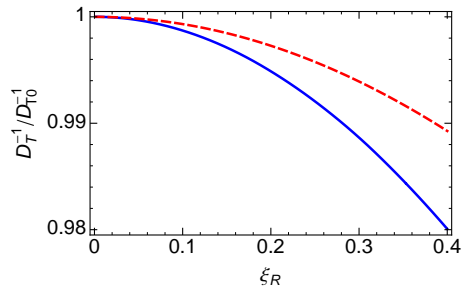


FIG. S2. Dependence of  $D_T^{-1}/D_{T0}^{-1}$  on the SIA magnitude measured in terms of  $\xi_R$ . Here  $D_T$  ( $D_{T0}^{-1}$ ) is the thermodynamic density of states obtained with (without) SIA for quantum-well width  $d = 7 \text{ nm}$  and  $n = 5 \times 10^9 \text{ cm}^{-2}$  (red dashed curve) and  $5 \times 10^{10} \text{ cm}^{-2}$  (blue solid curve).

quantum well [46]). Figure S2 illustrates the effect of SIA on  $D_T^{-1}$  in the inverted regime ( $d = 7 \text{ nm}$ ), demonstrating that SIA reduces  $D_T^{-1}$  only slightly and that the reduction is larger for higher densities. However, the relative change amounts to a few percent only. For the normal case ( $d = 5 \text{ nm}$ ), the change is even less than 1%.

*BIA.* The effect of BIA can be accounted for by augmenting the BHZ Hamiltonian, Eq. (3), by the term [29]

$$\mathcal{H}_\Delta = \begin{pmatrix} 0 & 0 & 0 & -\Delta \\ 0 & 0 & \Delta & 0 \\ 0 & \Delta & 0 & 0 \\ -\Delta & 0 & 0 & 0 \end{pmatrix}. \quad (\text{S2})$$

In Fig. S3, we plot the relative change of  $D_T^{-1}$  due to BIA in the inverted regime. The figure shows that BIA leads to an increase of  $D_T^{-1}$  by up to 15%, which further increases the difference between the magnitudes obtained for this quantity in the interacting and noninteracting cases. Also, in contrast to SIA, the effect of BIA is larger for smaller densities.

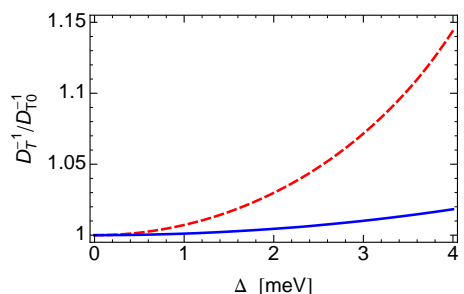


FIG. S3. Dependence of  $D_T^{-1}/D_{T0}^{-1}$  on the BIA magnitude  $\Delta$ . Here  $D_T$  ( $D_{T0}^{-1}$ ) is the thermodynamic density of states obtained with (without) BIA for quantum-well width  $d = 7 \text{ nm}$  and  $n = 5 \times 10^9 \text{ cm}^{-2}$  (red dashed curve) and  $5 \times 10^{10} \text{ cm}^{-2}$  (blue solid curve). In actual samples,  $\Delta = 1.8 \text{ meV}$  [27, 29].